Seismic-guided estimation of log properties

Part 3: A controlled study

By PHILIP S. SCHULTZ, SHUKI RONEN, MASAMZ HATTORI, PASCAL MANTRAN, CHIP CORBETT
Schlumberger (GeoQuest and Geco-Prakla)

In the first two parts of this series (published in the previous two issues of *TLE*), we discussed an alternative way of generating maps of rock or reservoir properties by using seismic attribute guidance. Normal procedure in generating such property maps (e.g., porosity, water or hydrocarbon saturation) takes the well data as control values, and uses 3-D seismic mainly for structural control. Using 3-D seismic attributes to guide the estimate of properties takes more effort, so there must be a reason that we choose to do it that way. In Part 1, we saw that property maps generated using attributes show greater detail. We also saw some theoretical considerations suggesting greater accuracy compared to maps from log data alone, but greater accuracy was not proven or demonstrated. Here we address the question *Are the maps really more accurate?* by reviewing the results of a controlled study.

We chose, for this study, a producing field with 15 logged wells and 3-D seismic data in a marine environment. This field was selected because it was producing significant hydrocarbons, because the seismic and log data were of high quality, because a uniform and comprehensive suite of log curves was available for each well, and because the number of logged wells was sufficient for an adequate level of statistical significance. The seismic guided property estimation method was applied to fields with a small number of wells, with a clear need for seismic guidance. In such fields, however, the statistical confidence is reduced. On the other hand, in fields with a large number of wells (more than 100), the statistical significance is larger, but the value of including seismic data in the property estimation is reduced because we know the reservoir much better.

The field and the data. The field consists of several producing layers. The study focused on a relatively shallow producing layer, called Oslo. Figure 2 from Part 1 shows a single-well view of several log tracks from the Diamond well, and includes a formation evaluation track and a track with geologic markers. The Oslo marker defines the top of the Oslo layer; the bottom is defined by the Paris marker.

The 15 wells are all deviated and

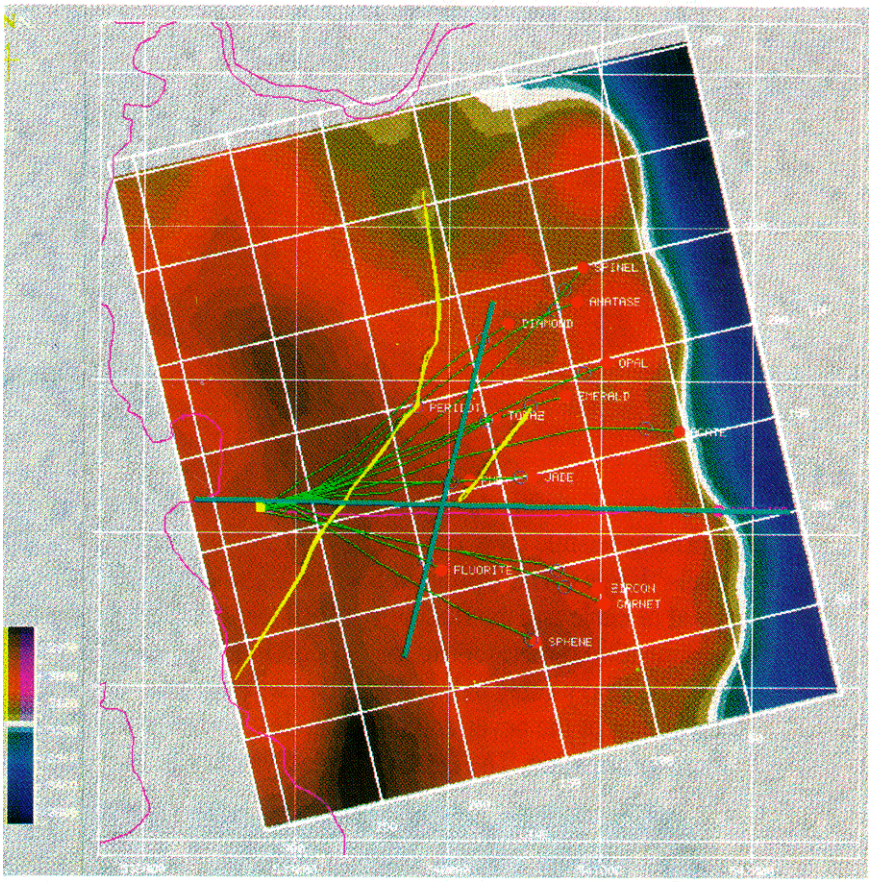

Figure 14. Fifteen named wells, originating from a single platform shown in yellow, provide the downhole data for the study. TD for each well is marked by solid red circles, and green open circles identify the intersection with the top of the Oslo layer. The background image gives the time structure of this layer, and includes two faults shown in yellow. The two oblique lines in blue, roughly east-west and north-south, indicate the location of the seismic sections in Figures 15 and 16, and are such that the projected wells intersect the seismic display at the approximate depth of the Oslo layer.

originate from the same platform. Wells originating from this platform all penetrate the Oslo layer, are all logged, and are all included in the study. The names of the wells, layers, horizons, and the values of time, depth, and UTM coordinates and the coastline shape have been modified. The phrase "well location" will refer to the map position of the intersection point of a given deviated well with the Oslo layer.

A good quality 3-D seismic data set was collected over this field with a north-northwest line orientation. The portion of this data set covering the platform and trajectories of all wells was used in the study. The 3-D subset comprises 3 15 lines and 360 CDPs. The figures show the relative positions and geometry of the wells, the platform, and the seismic data.

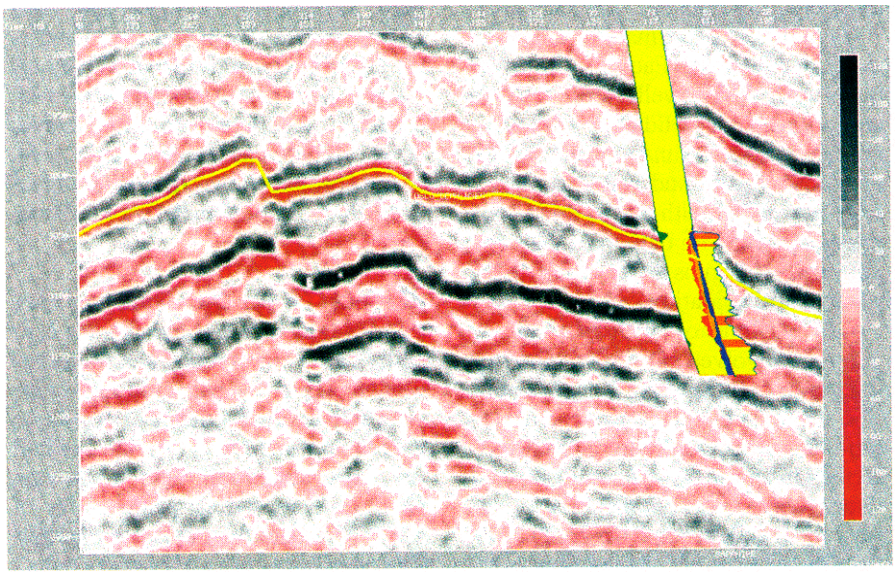

Figure 15. East-west line, with the Sapphire well projected on the display. To the left of the well trajectory are the formation evaluation curves, with shale in green, clean matrix in yellow, and moveable hydrocarbons in red. To the right is the lithofacies within the gamma ray curve. The yellow horizon is the interpreted top of the Oslo layer, and shows the major north-south fault. The seismic response of the full sequence of producing layers is evident below the Oslo horizon.

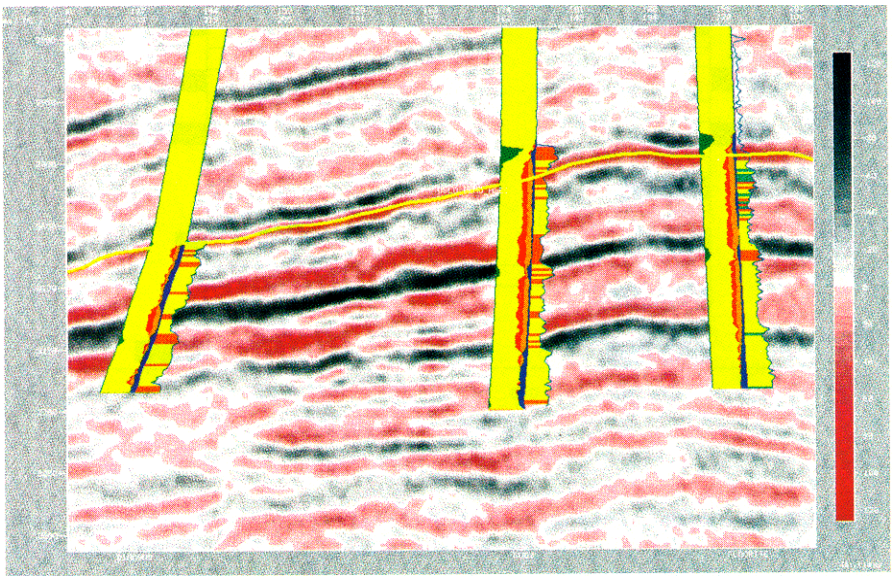

Figure 16. North-south line, with north to the left. The Diamond, Ruby, and Flourite wells are projected (from left to right). Log curves shown are the same as for Figure 15.

Data preparation. The 3-D data were processed through time migration in a standard manner. After migration, a residual phase correction filter was applied to the seismic data, based on a relative phase analysis between a synthetic trace at the Topaz well and a "deviated trace" extracted from the 3-D seismic data volume along the well trajectory. The relative phases of the two traces were compared in the vicinity of the Oslo layer. A single correction filter was estimated from this analysis, yielding a phase correction of about 60 degrees, and was applied to the entire 3-D data set in a spatially invariant manner.

Because a search for statistically significant spatial relationships between seismic attributes and rock properties would follow this filtering step, we chose to avoid a spatially-varying filter application driven by a multiwell phase analysis. In other words, if we used log property data (i.e., the density and sonic logs represented in the synthetic trace) to change the spatial variability of the seismic data in any way, statistical correlations subsequently found between the two data sets would be suspect. For this reason, the phase correction involved the application of a strictly spatially-invariant filter.

Following the residual phase correction filter application, a band-limited seismic impedance volume was computed from the seismic trace data alone. On each trace independently, a recursive calculation was made for acoustic impedance, assuming that the seismic trace was a band-limited reflectivity series, according to the relation

$$Z_i = Z_{i+1}\frac{1-R_{i,i+1}}{1+R_{i,i+1}}$$

where Z_i is the impedance in layer i, and $R_{i,i+1}$ is the reflection coefficient at the interface between layers i and $i+1$. This inversion to acoustic impedance was used as a seismic attribute. As such, it necessitated no merging with log data, even though we would normally do so to create the "best" seismic impedance section (particularly to include low frequencies). The reason, as before, is not to taint any statistical significance which might be found between the log

and seismic impedance attribute data. An impedance subvolume was then extracted between the two surfaces defining the Oslo layer, and vertical arithmetic averaging of the impedance was done, giving a grid of average impedance for the Oslo layer. This grid was used as the acoustic impedance attribute in the subsequent analysis.

A time horizon interpreted from the 3-D seismic data representing the top of the Oslo layer is shown in map view and on two oblique sections in the first three figures. Figure 14 shows the surface locations of the two lines, which trend approximately north-south and east-west. The lines were positioned so that the projected wells intersect the sections near the Oslo layer marker. Figures 15 and 16 show the east-west and north-south lines, with the top of the Oslo layer interpreted in yellow. These sections show a series of strong and coherent reflectors in the producing zone. The well data, displayed along the well trajectories on the sections, show that the Oslo layer, the subject of this study, is near the top of the sequence.

This horizon was converted to depth, and the resultant grid was subsequently used as an attribute. An average velocity grid was calculated by modeling seismic stacking velocities, and was followed by a residual correction using time-depth relationships from all 15 wells, derived from sonic logs calibrated by check shot and VSP data. The average velocity grid was then used to convert the time-based surface grid to a depth surface, further constrained by well ties to the top of the Oslo layer. As in the previous steps of residual wavelet processing and inversion, no rock property measurements from logs were used to change the spatial variation of the seismic attributes. The only log information used in this step were the time-depth curves.

Other attributes were computed. However, the only ones used in the study were impedance and depth.

Rock and reservoir property curves were computed from measured logs in a standard petrophysical analysis. The resultant property log curves included (among others) a volumetric analysis (component volume fractions), effective porosity, and log acoustic impedance. These processed curves were averaged arithmetically over a vertical zone defined by the top and bottom of the Oslo layer, as interpreted on log data from each of the 15 wells.

Data analysis. A statistical significance analysis was made on the attributes and log properties. The resulting quality matrix can be seen as Figure 4 in Part 1. For this study, we chose to estimate effective porosity guided by the acoustic impedance attribute (significance 81 percent) and water saturation guided by the depth attribute (significance 90 percent). The corresponding cross plots are Figures 5 and 6 in Part 1.

Five different estimation runs were made in the study. Each run followed this scenario: Six wells were selected and put aside as validation wells (i.e., not used in the estimation procedure); maps of porosity and water saturation were estimated, with and without seismic guidance, with data from the other nine wells. The runs differed only in the selection of validation wells.

The estimation *without* attribute guidance involved simply gridding the log property values from the nine wells. The estimation *with* seismic attribute guidance followed the method described in Part 1. A linear attribute calibration curve was computed as a best least squares fit through the points from the nine wells in the attribute-property cross plot, followed by a residual correction step, also using data from only the nine included wells. The same gridding (mapping) algorithm was used for all gridding steps. For each estimation run, four grids (maps) were generated: effective porosity and water saturation, each with and without seismic attribute guidance.

The depth-averaged log values for porosity and water saturation at each of the validation wells were then compared to predicted values from maps made with and without seismic guidance. The signed estimation error in a given validation well was computed as the log property value in that well minus the grid value of that property at the well location. Average estimation errors were computed as the arithmetic mean of the absolute values of the individual estimation errors from the six validation wells.

Results. Of the five estimation runs, four resulted in a reduced average estimation error for porosity and water saturation. The best result gave an average error reduction of a factor of about two for porosity and about two and one half for water saturation. The worst case gave an increased estimation error of about 3 percent for the two properties. The other three runs all showed a reduction in the estimation error.

In the best case, the magnitudes of the estimation errors were reduced for each of the six validation wells (Figure

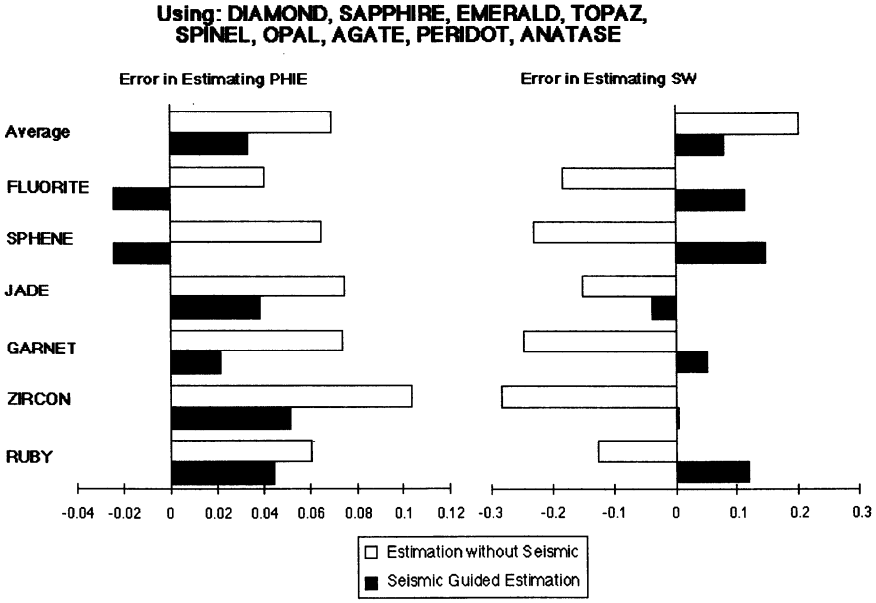

Figure 17. A comparison of estimation errors at each of the six validation wells for effective porosity (left) and water saturation (right) for estimates done with (solid bars) and without (open bars) seismic guidance. The seismic guided procedure has reduced the magnitude of the estimation error averaged over all six wells, shown in the top bar, by a factor of about 2 for porosity and about 2 1/2 for water saturation.

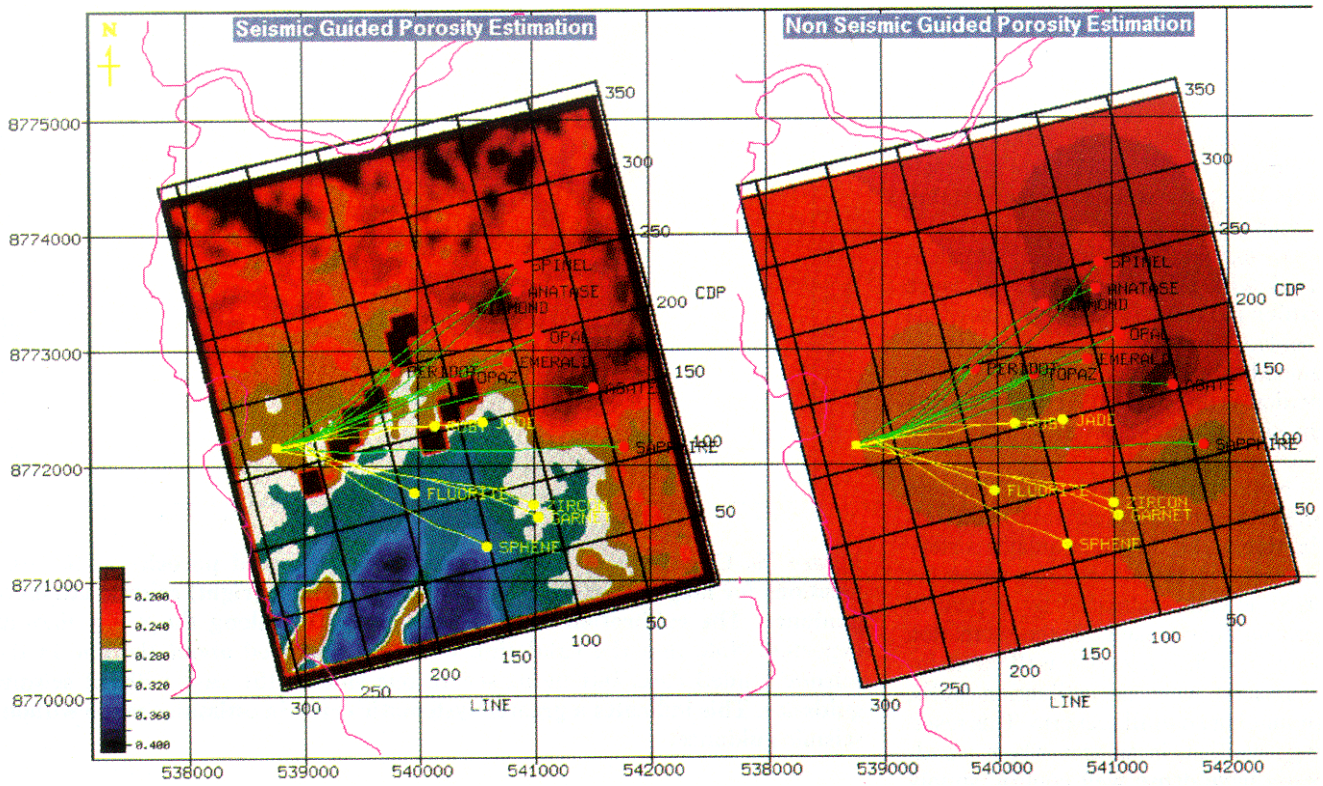

Figure 18. Maps of porosity made from the nine calibration wells (green and red) with (left) and without (right) seismic attribute guidance. Validation wells are in yellow. Well names are displayed on the base maps next to TD (solid circle). Map values agree at the calibration wells in both methods, but differ at the validation wells. Black rectangles in the seismic guided map show areas near faults where the attribute values were absent. The color scale at the lower left shows the correspondence of color to porosity. The seismic guided map is two times as accurate in predicting porosity values at the yellow ("unknown") validation wells.

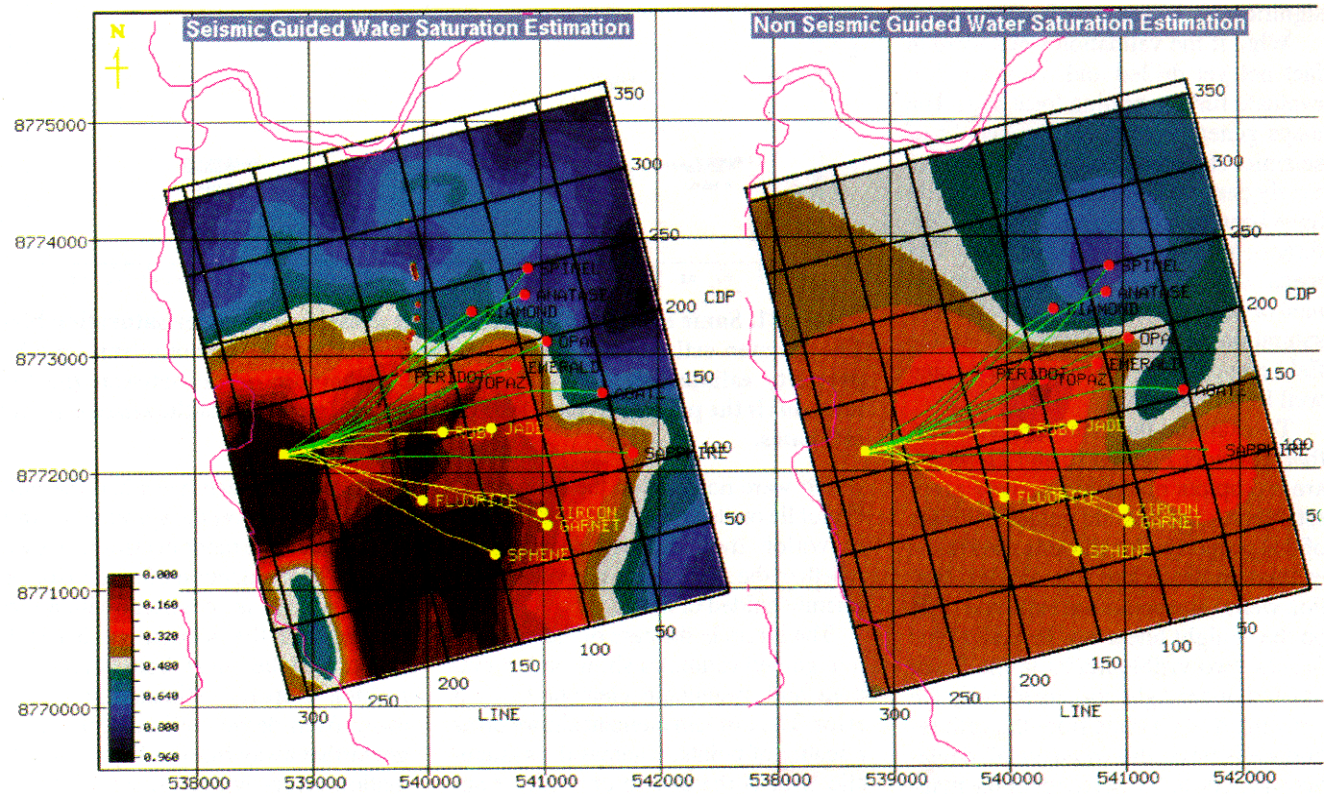

Figure 19. Same as Figure 18 but showing maps of water saturation. The seismic guided map is two and one half times as accurate in predicting water saturation values at the validation wells.

17). Figures 18-19 show the property distribution maps for porosity and water saturation, with and without seismic guidance, resulting from this run. The wells and trajectories in yellow are the validation wells. Each map in a pair shares the same color scale representing property values.

As expected, the distributions calculated with seismic attribute guidance exhibit more detail. Also, because of the residual correction step, the seismic guided estimates agree at the nine calibration wells, as do the estimates from the simple gridding run (without seismic guidance).

Notice that the validation wells were all grouped together, apart from the calibration wells, which simulates a step-out scenario. In the worst run, where the error actually increased by 3 percent (essentially no change in the estimation accuracy), the validation wells were interspersed with the calibration wells, simulating an infill scenario. This result suggests that, in an area where we already have dense well control, simply gridding the control values from the known wells may give results that are just as accurate. On the other hand, where we are looking to predict reservoir or rock property behavior away from areas of dense well control, seismic guided log property mapping can significantly increase map accuracy.

What if the validation wells were in fact not yet drilled and we wanted to evaluate further drilling locations? The maps generated without the benefit of seismic attribute guidance would be overly pessimistic. (They could equally have been overly optimistic with a different choice of validation wells.) The maps with seismic guidance show an area of higher porosity and lower water saturation in the southern part of the field compared to the maps made using well information only.

To examine the error behavior further, consider Figures 20 and 21, which are crossplots of the log-derived property versus the seismic guided estimate of that property. For all wells used in the estimation procedure (the nine calibration wells), the points are expected to lie on the straight line x = y. In each of the frames, two visible marks in the lower left and upper right comers identify the x = y trend. All points from the calibration wells lie on this trend (small deviations are due to the behavior of the mapping algorithm and the finite grid spacing). However, the validation wells,

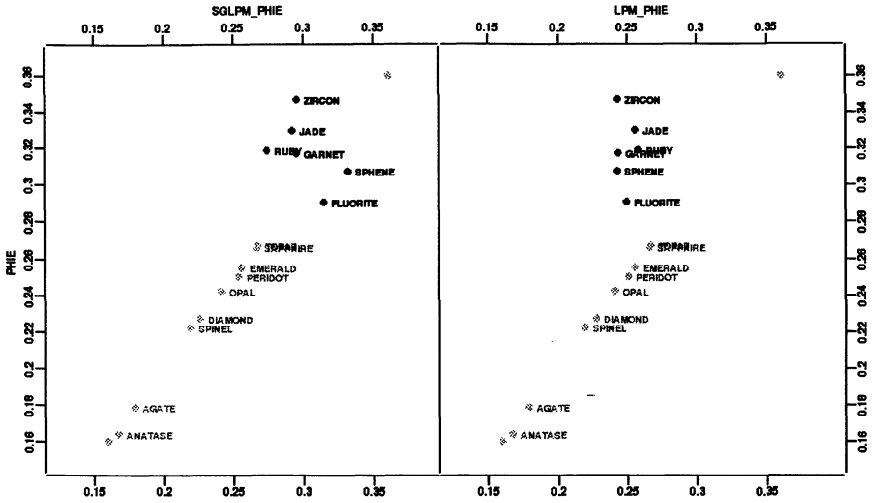

Figure 20. Crossplots of log porosity versus estimated porosity at the well locations for maps generated with (left) and without (right) seismic attribute guidance. The calibration wells lie approximately along the x = y line, as expected. Note that the validation wells are scattered about the line in the seismic guided case, but lie biased to one side in the case without seismic guidance. This indicates a greater systematic error in estimates made without seismic guidance.

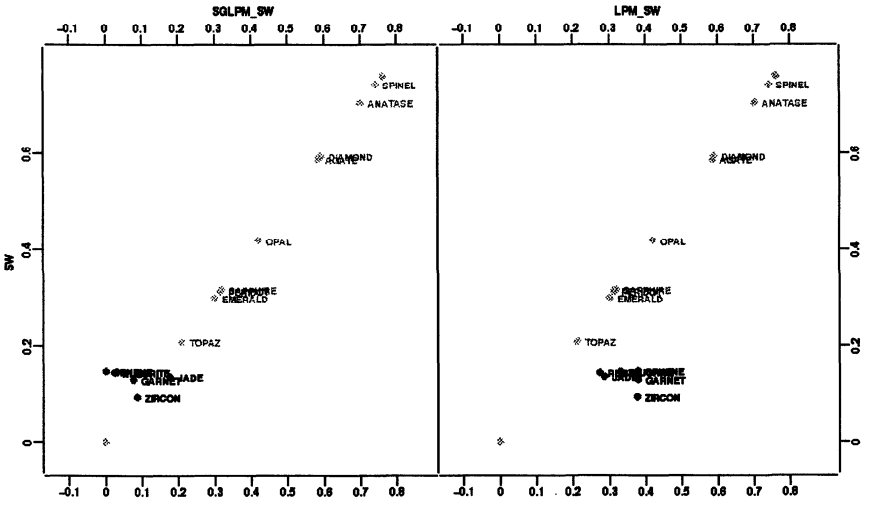

Figure 21. Same as Figure 20 but showing crossplots of water saturation bias. The greater estimation bias can be seen in the case of nonseismic guided property estimation. This difference in systematic error between the two methods is the principal reason for the increased accuracy of the seismic guided estimates.

which were not used in the estimation, do not lie on the x = y trend, and the way in which they deviate depends on whether the estimation procedure was seismic guided or not.

The errors in the case of the nonseismic guided estimates show both a random and systematic element to their error. The random element shows up as a scatter of points, whereas the systematic error is the bias to one side or another of the points from the desired trend line. Applying seismic guidance to the property estimates had the most dramatic effect on the systematic error, but affected the random error to a lesser extent. This reduction of systematic estimation error is consistent with a conclusion that the seismic guided technique will be most beneficial when making property estimates in an area away from dense well control. As we get farther away from well control, estimation errors will be dominated by a reduced ability to predict accurately the general trend in the behavior of the

property distribution. When this occurs, the character of the map is driven more by the details of the mapping algorithm than by the data control points. Such systematic errors can become very large.

The remaining figures are maps generated from estimates using data from all 15 wells. Figures 22 and 23 show maps of porosity estimates with and without seismic guidance. Water saturation maps are represented in the same way in Figures 24 and 25. Because no wells were withheld in the calibration, the property values from logs (porosity or water saturation) agree with the gridded property values at the map locations. The differences lie in the level of detail and in the predicted property values away from well control.

Both techniques predict a higher porosity zone to the south and west, but there is disagreement in the distribution of porosity north of the platform.

The seismic-guided water saturation map using all 15 wells (Figure 24) looks very similar to the seismic guided estimate made with only the nine wells in the controlled study (Figure 19). On the other hand, the maps made using only well data show a significant difference when using the full suite of wells rather than only nine (Figures 25 and 19), implying again that seismic guidance can sometimes make up for lack of well control.

There is notable disagreement between the seismic guided and wells-only estimates of the distribution of water saturation using all 15 wells (Figures 24 and 25); the seismic-guided estimate predicts lower water saturation in the vicinity and to the west of the platform. Coupled with the predicted high porosity from the map of Figure 23, seismic-guided property estimation suggests this area as a promising location for further development of this producing layer. The wells-only map does not highlight this location to the same degree.

Seismic-guided log property estimation, as a new way of using seismic data to make maps of rock and reservoir properties, is a departure from standard procedure of mapping properties from log values only. Theoretical considerations (in Part 1) and the results of controlled studies (as the one discussed in this part) suggest a simple but profound conclusion: *We get better estimates of the distribution of rock and reservoir properties away from well control when using seismic attribute guidance.*

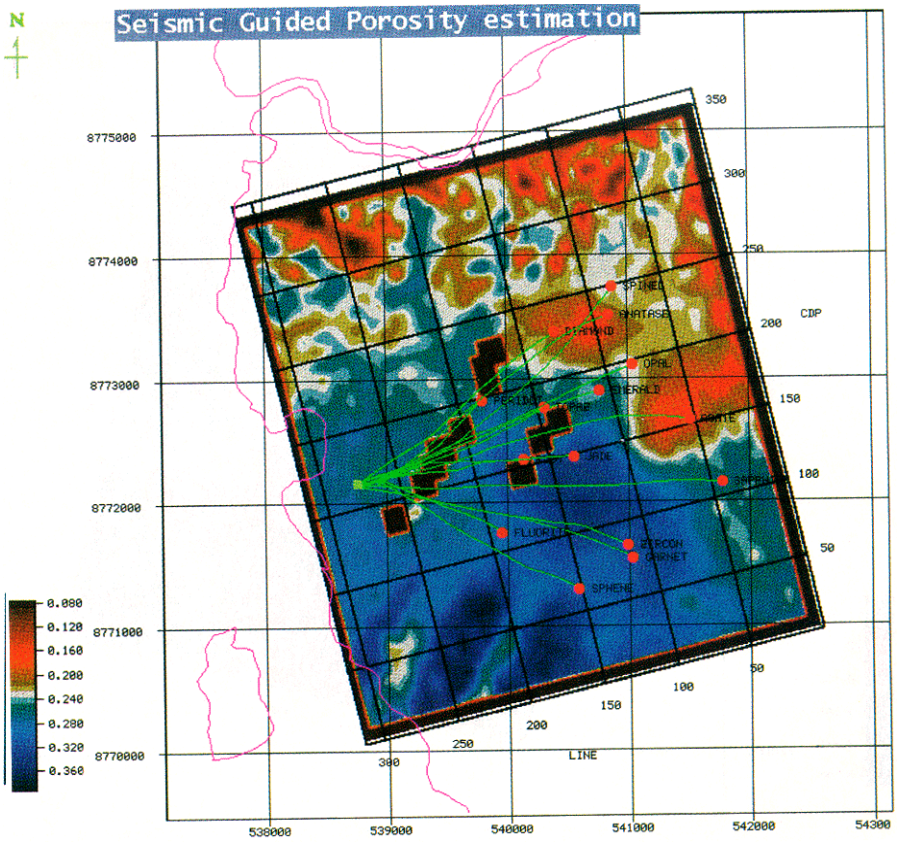

Figure 22. Map showing the estimate of the property distribution using seismic attribute guidance and log data from all 15 wells.

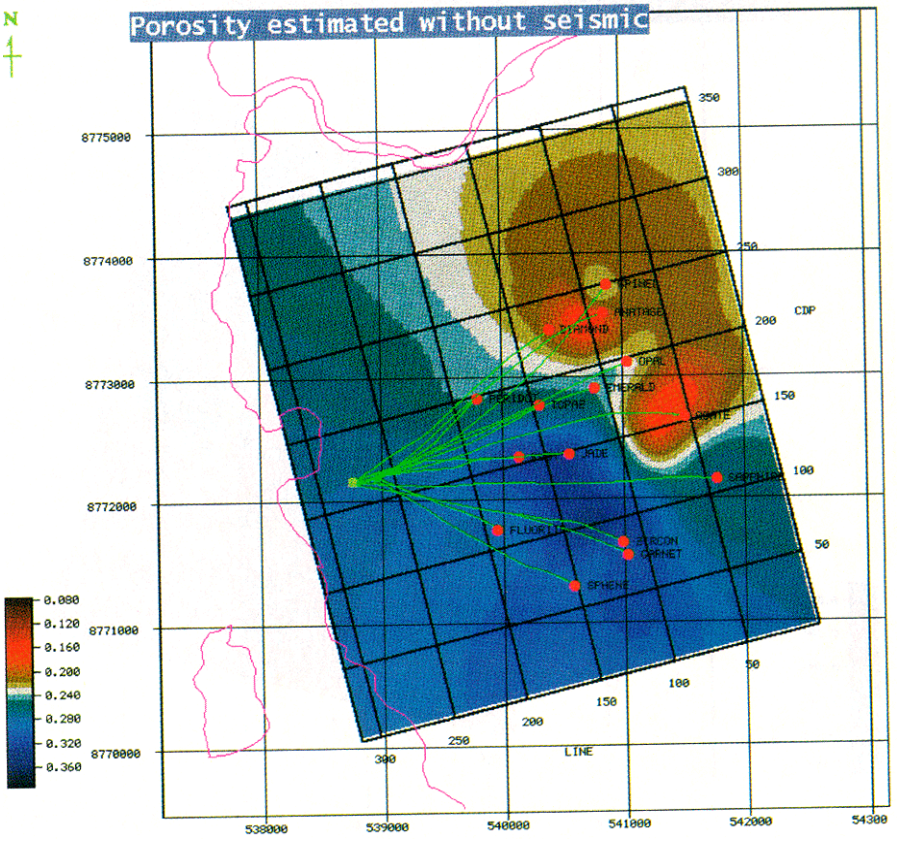

Figure 23. Porosity map using only log data from the 15 wells.

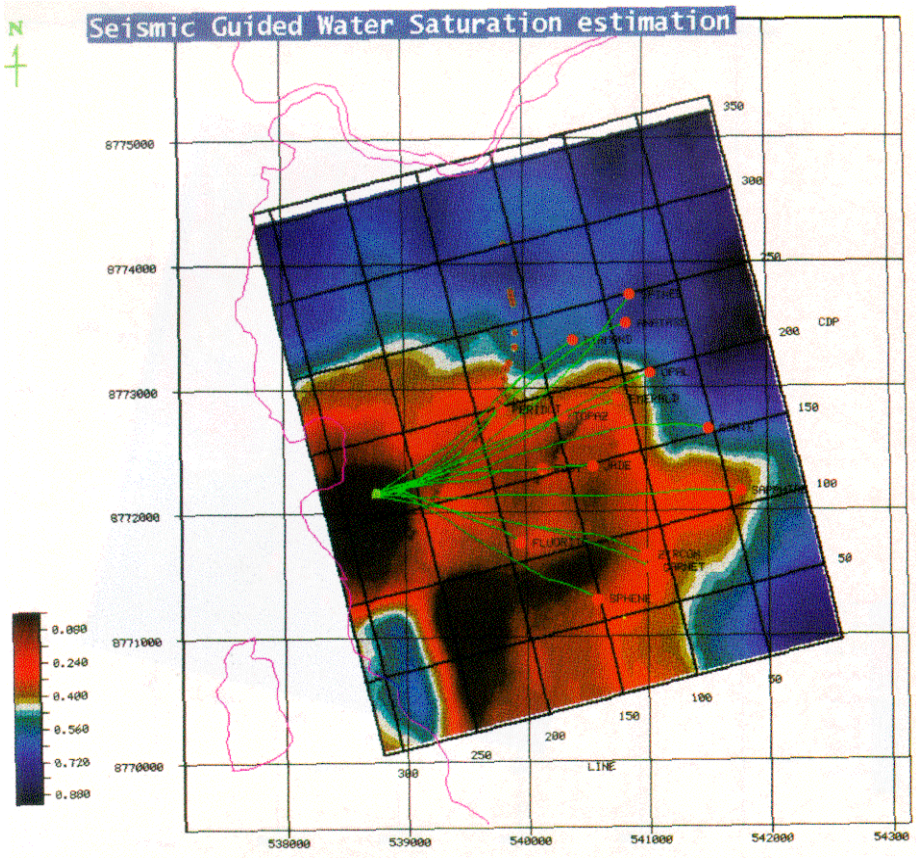

Figure 24. Map showing the estimate of water saturation distribution using seismic attribute guidance and log data from all 15 wells.

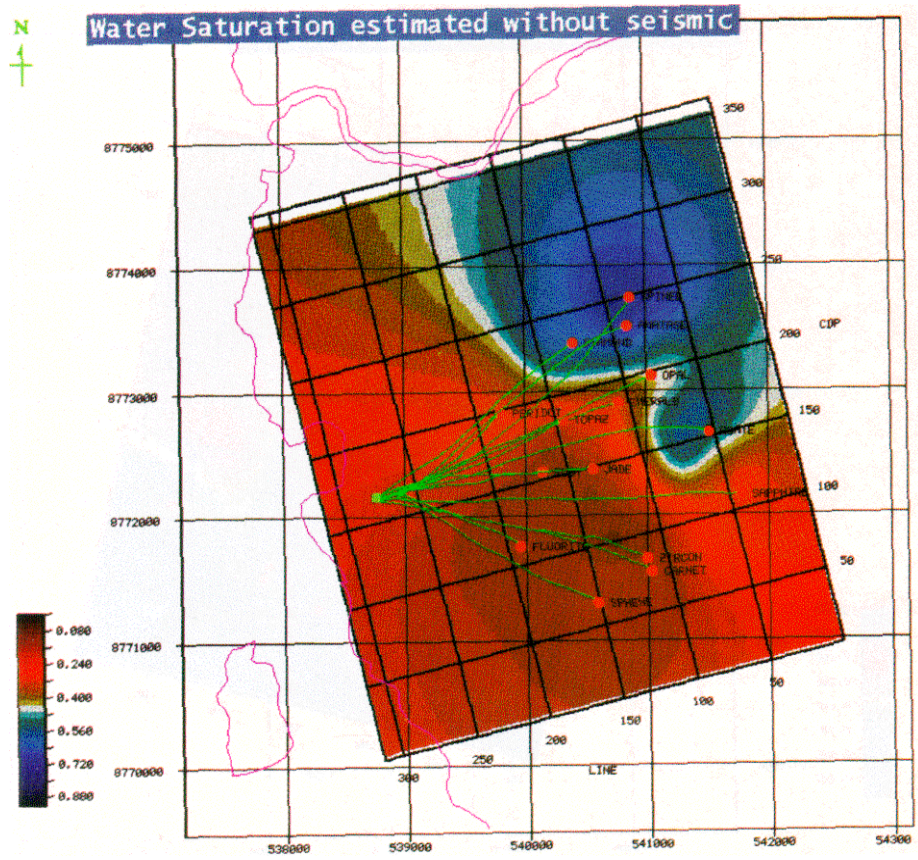

Figure 25. Water saturation map using only log data from the 15 wells.

Because it is a data-driven method, this estimation procedure requires a systematic attribute-versus-property analysis, looking for statistically valid relationships, prior to the seismic guided mapping. Even with such a prior analysis, seismic guided estimates can range from providing either dramatically improved predictions (as in the stepout scenario of the controlled study) to giving essentially no improvement (as in the infill scenario) depending on the data.

While rock physics relationships provide the underlying link between seismic attributes and log properties, such links can be obscure and be difficult or impossible to derive theoretically from first principles. The seismic response depends on many variables, including volume of clay, pressure and temperature, nature and geometry of the subwavelength layering, overburden transmissivities, and other factors which affect elastic and absorption response. These complex relations can vary from one layer to another, and even within a single layer or reservoir compartment. Add to that the variability in data processing and we are in a position of often needing to know impossibly many fine details of the medium and the processing before we can derive theoretically the seismic response in sufficient detail to predict the same attribute-property relationships that manifest themselves clearly in the methodology used in this study.

We can generally improve both the accuracy (ability to predict) and spatial resolution (detail) of our property maps. The key is the use of 3-D seismic with log data in a systematic data-driven analysis. LE

Acknowledgements: Part 1 (May 1994 TLE)- We thank Clement Kostov and Gilles Mathieu for sharing their insights 072 geostatistical methods. Peter van Bemmel, Bobbie Ireland, and Linda Salinsky offered suggestions to improve the manuscript. Part 2 (June 1994 TLE) -We enjoyed having many fruitful discussions with Josiah Hoskins, a real expert 071 ANNS. He supplied us with several key routines for incorporating this technique in a workstation setting. Guillermo Arango and Jahir Pabon of the Schlumberger Laboratory for Computer Science critically reviewed the manuscript.